Nonlinear Dynamics and Applications: Proceedings of JIPNR-Sosny. Vol. 31 (2025) 122 - 139

Calculations of the Sixth-Order QED Corrections to Lepton Anomalies due to the Fourth Order Vacuum Polarization Insertions

L.P. Kaptari,[1,*] V.I. Lashkevich,[2,†] and O.P. Solovtsova[1,2,‡]

[1] *Bogoliubov Lab. Theor. Phys., JINR, Dubna, 141980, Russia*

[2] *Gomel State Technical University, Gomel, 246746, Belarus*

The explicit form of the sixth order radiative corrections to the lepton L ($L = e$, μ and τ) anomalous magnetic moment from QED Feynman diagrams with insertion of fourth-order polarization operators, consisting either on two closed lepton loops or one lepton loop crossed by a photon line, is discussed in details. The approach is based on the consistent application of dispersion relations for the vacuum polarization operators and the Mellin–Barnes transform for massive photon propagators. Explicit analytical expressions for the corrections to the lepton anomaly are obtained in the whole interval $0 < r < \infty$ of the ratio r of lepton masses m_ℓ/m_L. Asymptotic expansions are computed in the limit of both small $r \ll 1$ and large $r \gg 1$ and found to be in a perfect agreement with the ones early reported in the literature. We argue that in the region where the physical ratios are located, the asymptotic expansions hold with an accuracy higher that the experimentally measured anomalies.

PACS numbers: 12.20.-m,13.40.Em, 12.20.Ds, 14.60.Ef

Keywords: anomalous magnetic moment of leptons, radiative corrections, Feynman diagrams, Mellin–Barnes representation

1. Introduction

The anomalous magnetic moment of the electron and muon is now one of the most precisely measured quantities in particle physics and allows one to thoroughly test the relativistic local Quantum Field Theory (QFT) with tremendous accuracy. The physics of the gyromagnetic factor g_L, defined as the ratio between the magnetic moment μ and the spin s of a lepton L with charge e and mass m ($\vec{\mu} = g_L \frac{e}{2m}\vec{s}$), has challenged the particle physics community since long time and experiments as well as theory in the meantime look rather intricate. Its significance is tightly connected with its early role as a valuable test of QFT. Dirac's relativistic theory of quantum mechanics remarkably predicted that the g_L-factor of a free, point-like fermion should be exactly 2, see Ref. [1]. However, latter on J. Schwinger [2] computed the leading-order quantum correction to the lepton magnetic moment, arising from the self interaction with a virtual photon, and found a small correction $\sim \alpha/2\pi$, where α is the electromagnetic fine structure constant, which explained the unexpected $\sim 0.12\%$ excess observed in precision measurements of the electron's magnetic moment, a discrepancy referred to as the anomalous magnetic moment of the electron. This success served as additional argument in foundation of Quantum Elec-

*E-mail: kaptari@theor.jinr.ru

†E-mail: lashkevich@gstu.gomel.by

‡E-mail: solovtsova@gstu.gomel.by;olsol@theor.jinr.ru

trodynamics as the true, authentic theory of the electromagnetic interactions, and QFT as a general framework for the theory of elementary particles. It is now conventional to define the anomalous magnetic moment of a fermion L as $a_L = (g_L - 2)/2$ (see, e.g. Refs. [3, 4]), which quantifies the deviation of g_L from the Dirac value of 2. Since then, the anomalous magnetic moment have been measured with incredible accuracy becoming the best measured quantity in the Standard Model (SM) and allows one to test relativistic local Quantum Field Theory (QFT) with unprecedented accuracy. It puts severe limits on deviations from the standard theory of elementary particles and investigations of the anomalous magnetic moments has challenged the particle physics community for long time now and experiments as well as theory look hitherto highly topical. The magnetic momenta a_μ and a_e provide the most precise tests of QED in particular and of relativistic local QFT as a common framework for elementary particle theory in general. Presently, the electron's g-factor is known with an accuracy of 0.13 ppb, and the muon's g-factor with an accuracy of 0.19 ppm(for a update of the muon anomaly in the SM, see Ref. [5]), e.g. $\sim 10^{-10}$ for electrons [6] and 10^{-6} for muons [7]. These measurements, along with the corresponding theoretical calculations at high orders, are aimed on probing the limits of the SM or possible existence of as yet undiscovered particles belonging to SM, however giving rise to some "new physics" (NP) which still causes hunting for deviations of experiment from theory. Given the exceptional susceptibility to NP, uncertainties on the SM prediction should be reduced to the same level as the experimental ones to maximize the reliability in interpretation of data. In the SM, a_L is calculated from a perturbative expansion in the fine-structure constant α. The most important contributions to α_L arise from pure QED diagrams, but starting from the order α^2 also hadronic contributions, in particular hadron vacuum polarization and hadron light-by-light scattering, become notable. Nowadays the high precision calculations of QED corrections (up to the fifth order in α) are performed by means of special computational algorithms, e.g. the high-precision calculation by difference equations [8, 9], augmented by the PSLQ-algorithm [10]. These methods assure several hundreds or even thousands significant digits in final results [8, 9]. In spite of the ability to perform so high precision calculations, these approaches turn to be quite cumbersome in practice application. Even in case of parallel computation realisation, one requires a huge amount of computer time. Moreover, due to cumbersomeness of the method, a detailed analysis of the results with separate investigation of the role of particular type of diagrams, as well as independent confirmation of the numerical results appear to be rather awkward. In this context, it is quite tempting to identify in the full set of diagrams of a given order a subgroup of specific diagrams which enable close analytical calculations. This subgroup consists exclusively of diagrams with insertions of the vacuum photon polarization operator with inclusion of self-energy corrections of the corresponding order. The simplest type of such operators is the one consisting solely of closed lepton loops, usually referred to as the "bubble" -like diagrams. Based on the Mellin-Barns representatioln for the massive propagators (see. Ref. [11] for details), the lepton anomalies a_L for this type of diagrams have been calculated analytically up to the tenth order, cf. Refs. [11–13]. The next in complexity operators are the diagrams with closed lepton loops crossed by photon lines referred in what follows to as the "mixed" type. Obviously, the lowest order of mixed diagrams is α^2 and contributes to the sixth and higher orders radiative corrections to a_L. In this paper we focus mainly on analytical calculations of the sixth order corrections stipulated by accounting for only one mixed loop in to the vacuum polarization operators. This is a natural extension of our early calculations of corrections from the bubble-like diagrams [13, 14] where the corresponding analytical expressions were obtained as functions of the mass ratios $r = m_\ell/m_L$ of the loop lepton ℓ to the external one L, in the whole region $0 < r < \infty$. As before, our consideration is based on a combined use of the dispersion relations for the polarization operators

and the Mellin-Barnes integral transform for the Feynman parametric integrals. It should be noted that first explicit calculations of mixed diagram were reported in Ref. [15] in the asymptotic limits $r \ll 1$ and $r \gg 1$. Herebelow, our efforts are aimed on exact calculations of the mixed diagrams for any value of r, $0 < r < \infty$.

2. Vacuum polarization and the lepton anomaly

In this section we present the most general expressions for the vertex radiative corrections from diagrams with vacuum polarization insertions. The particular case when the vacuum polarization operator consists only on closed lepton loops was previously considered in details in Refs. [13, 14, 16]. Here below we consider a more complicate polarization operator which includes also loops with internal photon lines. The renormalized photon propagator can be written as

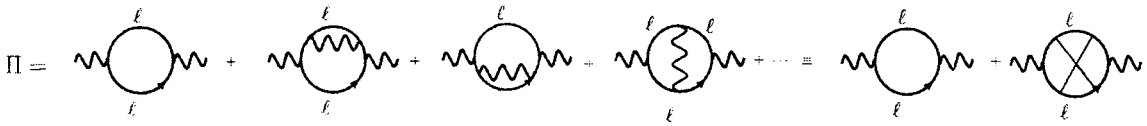

Figure 1: The irreducible proper graphs contributing to the vacuum polarization operator up to the fourth order. The crossed loop is the shorthand notation for the sum of diagrams with one internal photon line.

$$D_{\alpha\beta}(k^2) = -ig_{\alpha\beta}\frac{1}{k^2}\frac{1}{1+\Pi(k^2)} =$$
$$-ig_{\alpha\beta}\frac{1}{k^2}\left[1-\left(\Pi(k^2)-\Pi^2(k^2)+\Pi^3(k^2)+\cdots\right)\right] \equiv -ig_{\alpha\beta}\frac{1}{k^2}\left[1-\widetilde{\Pi}(k^2)\right], \qquad (1)$$

where $\Pi(k^2)$ is the sum of all the irreducible self-energy graphs which, up to the fourth order, are depicted in Fig. 1. The quantity $\widetilde{\Pi}(k^2)$ in Eq. (1) includes all powers of the irreducible graphs,

$$\widetilde{\Pi}(k^2) = \Pi(k^2) - \Pi^2(k^2) + \Pi^3(k^2) + \cdots, \qquad (2)$$

which obviously contains all orders of the radiative corrections. For instance, the powers of the first diagram in Fig. 1 generates the series of the "bubble-like" graphs, labeled as a), b) and d) in Fig. 2 (see also Refs. [13, 14]). The diagram with crossed loops induces the so-called "mixed-bubble" types, cf. diagrams c) and e), which certainly determine the sixth and higher orders of the radiative corrections. The simplest diagrams of this type are depicted in Fig. 3.

As demonstrated in Refs. [4, 13, 14, 17] the vertex diagrams with insertion of only vacuum polarization operators can equivalently be represented by a diagram of the second order with exchange of one but massive photon. For this type of diagrams the lepton anomaly $K_L^{(2)}(t)$ is well-known in the literature [18–20] and reads as

$$K_L^{(2)}(t) = \frac{\alpha}{\pi}\int\limits_0^1 dx\,\frac{(1-x)x^2}{x^2+t(1-x)/m_L^2}, \qquad (3)$$

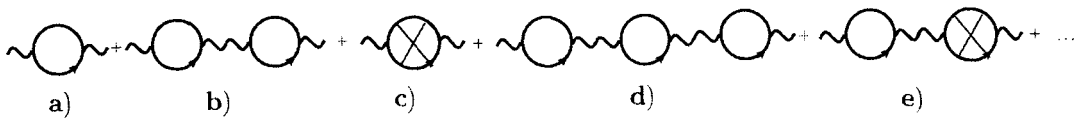

Figure 2: The possible combinations of the irreducible diagrams contributing to up to the sixth order vacuum polarization operator. Diagrams a), b) and d) are of the purely bubble-type diagrams, whereas diagrams c) and e) are of the so-called "mixed type", cf. Fig. 1.

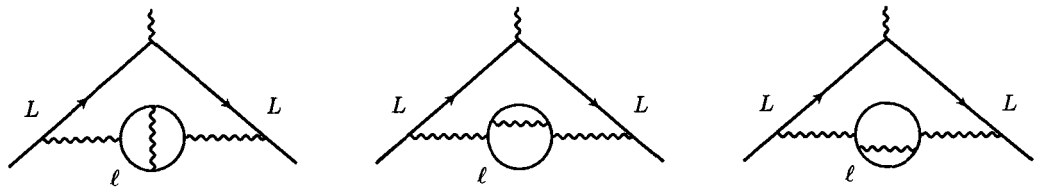

Figure 3: The simplest diagrams with insertions of the vacuum polarisation operator of the fourth order with one internal photon line. The external photon is labeled by "L", whereas the internal lepton in the loop is denoted as "ℓ".

where m_L is the mass of the scrutinized lepton, α is the fine structure constant. In what follows, throughout this paper the external lepton, as well as the loop leptons of the same kind as the external ones, are denoted by the capital letter L. The loop leptons, different from L, are denoted by the lowercase ℓ.

With Eq. (3), the anomaly a_L can be written as [4, 13, 14, 17]

$$a_L = \frac{1}{\pi}\int \frac{dt}{t}\mathrm{Im}\widetilde{\Pi}(t)K_L^{(2)}(t) =$$

$$= \frac{1}{\pi}\int \frac{dt}{t}\mathrm{Im}\widetilde{\Pi}(t)\frac{\alpha}{\pi}\int dx\frac{x^2(1-x)}{x^2+(1-x)t/m_L^2} = -\frac{\alpha}{\pi}\int\limits_0^1 dx(1-x)\tilde{\Pi}\left(\frac{-x^2}{1-x}m_L^2\right). \quad (4)$$

In obtaining Eq. (4) the dispersion relations for the operator $\Pi(t)$ have been employed. In the present paper we consider the polarization operator consisting on only two types of internal leptons, L and ℓ. The diagrams with three different leptons, L, ℓ_1 and ℓ_2 will be presented elsewhere. Generally, the polarization operator (2) for Feynman diagrams with insertions of $n = p + j$ closed loops, where p and j denote the number of lepton loops of L and ℓ kinds, respectively, can be presented as (q.v. Eq. (2))

$$\Pi^n(k^2) = \sum_{p=0}^{n}(-1)^{n+1}C_n^p\left[\Pi^{(L)}(k^2)\right]^p\left[\Pi^{(\ell)}(k^2)\right]^{j=n-p} \equiv \sum_{p=0}^{n}F_{(p,j)}\left[\Pi^{(L)}(k^2)\right]^p \times\left[\Pi^{(\ell)}(k^2)\right]^{j=n-p}, \quad (5)$$

where C_n^p are the familiar combinatorial coefficients and the quantity $F_{(p,j)} = (-1)^{p+j+1}C_{p+j}^p$ has been introduced as to reconcile our formulae with the commonly adopted notation, e.g., in Refs. [13, 14, 16]. Inserting Eq. (5) in to Eq. (4) and applying again the dispersion relations to $\Pi^{(\ell)}(q_{eff}^2)/q_{eff}^2$, where $q_{eff}^2 = -\frac{x^2}{1-x}m_L^2$, the corrections

$a_L^{(p,j)}$ to the anomaly a_L from diagrams with $p+j$ loops read as

$$a_L^{(p,j)} = F_{(p,j)}\frac{\alpha}{\pi}\int\limits_0^\infty \frac{dt}{t}\int\limits_0^1 dx \frac{x^2(1-x)}{x^2+(1-x)t/m_L^2}\left[\Pi^{(L)}\left(-\frac{x^2}{1-x}m_L^2\right)\right]^p \frac{1}{\pi}\,\mathrm{Im}\left[\Pi^{(\ell)}(t)\right]^j. \tag{6}$$

To further proceed with analytical calculations, we considers the integrand in Eq. (6) as the subject of the Mellin–Barnes transform, see e.g. Refs. [7, 20–22],

$$\frac{x^2(1-x)}{x^2+(1-x)t/m_L^2} = \frac{1}{2\pi i}\int\limits_{c-i\infty}^{c+i\infty} ds\left(\frac{4m_\ell^2}{t}\right)^s\left(\frac{4m_\ell^2}{m_L^2}\right)^{-s} x^{2s}(1-x)^{1-s}\,\Gamma(s)\Gamma(1-s), \tag{7}$$

where $0 < c < 1$ determines the strip in the complex plane of s along which the integrand (7) is an analytical function; the factor $4m_\ell^2$ has been introduced for further convenience. By virtue of the representation (7), we can write $a_L^{(p,j)}$, Eq. (6), as

$$\begin{aligned} a_L^{(p,j)} &= \frac{\alpha}{\pi}\frac{1}{2\pi i}F_{(p,j)}\int\limits_{c-i\infty}^{c+i\infty} ds\left(\frac{4m_\ell^2}{m_L^2}\right)^{-s}\Gamma(s)\Gamma(1-s)\int_0^1 dx\, x^{2s}(1-x)^{1-s} \\ &\times\left[\Pi^{(L)}\left(-\frac{x^2}{1-x}m_L^2\right)\right]^p\int_0^\infty\frac{dt}{t}\left(\frac{4m_\ell^2}{t}\right)^s\left(\frac{1}{\pi}\mathrm{Im}\left[\Pi^{(\ell)}\left(\frac{4m_\ell^2}{t}\right)\right]^j\right). \end{aligned} \tag{8}$$

Hence, the Mellin–Barnes transform made it possible to present the contribution to the lepton anomaly from different kinds of lepton loops in the following factorized form of two Mellin momenta

$$a_L^{(p,j)} = \frac{\alpha}{\pi}\frac{1}{2\pi i}F_{(p,j)}\int\limits_{c-i\infty}^{c+i\infty} ds\left(\frac{4m_\ell^2}{m_L^2}\right)^{-s}\Gamma(s)\Gamma(1-s)\,\Omega_p(s)R_j(s), \tag{9}$$

where

$$\Omega_p(s) = \int_0^1 dx\, x^{2s}(1-x)^{1-s}\left[\Pi^{(L)}\left(-\frac{x^2}{1-x}m_L^2\right)\right]^p, \tag{10}$$

$$R_j(s) = \int\limits_{4m_\ell^2}^\infty\frac{dt}{t}\left(\frac{4m_\ell^2}{t}\right)^s\frac{1}{\pi}\mathrm{Im}\left[\Pi^{(\ell)}\left(\frac{4m_\ell^2}{t}\right)\right]^j = 2\int_0^1\delta d\delta(1-\delta^2)^{s-1}\frac{1}{\pi}\mathrm{Im}\left[\Pi^{(\ell)}(\delta)\right]^j. \tag{11}$$

Here the variable is $\delta = \sqrt{1-4m_\ell^2/t}$.

Equations (9)-(10) represent the most general expressions for the lepton anomaly from diagrams with vacuum polarization operators consisting on leptons loops of two types, L and ℓ. Note that, in our previous papers we considered only irreducible diagrams of the second order, i.e. pure closed lepton loops. In that case for better illustration of the $2(p+j+1)$ orders of corrections, the factors $\left(\frac{\alpha}{\pi}\right)^p$ and $\left(\frac{\alpha}{\pi}\right)^j$ were emphasized explicitly in definitions of $\Omega_p(s)$ and $R_j(s)$. Since in the present paper we consider also one-loop polarization operators of the fourth order, the indices p and j do not longer illustrate unambiguously the order of the corrections. For this reason we include the factors $\left(\frac{\alpha}{\pi}\right)^p$ and $\left(\frac{\alpha}{\pi}\right)^j$ into the definition of the Mellin momenta and, instead, the order

of the correction we indicate by a subscript index for the corresponding polarization operators.

As seen from Eq. (11) the Mellin momentum $R_j(s)$ is manifestly independent on the lepton masses. The momentum $\Omega_p(s)$ depends only on the polarization operator $\Pi^{(L)}(q^2)$ for which the genuine variable is the dimensionless combination $\frac{4m_L^2}{q^2}$. It implies that, in our case $\Pi^{(L)}\left(-\frac{x^2}{1-x}m_L^2\right) = \Pi^{(L)}\left(-\frac{4(1-x)}{x^2}\right)$, i.e. $\Omega_p(s)$ also is independent on the lepton masses. Consequently, the only dependence on masses in $a_L^{(p,j)}$, Eq. (9), enters trough the ratio m_ℓ/m_L, which justifies the commonly adopted classification of $a_L^{(p,j)}$) as [3, 23]

$$a_L = A_{1,L}\left(\frac{m_L}{m_L}\right) + A_{2,L}\left(\frac{m_\ell}{m_L}\right) + A_{3,L}\left(\frac{m_\ell}{m_L}, \frac{m_{\ell_2}}{m_L}\right), \tag{12}$$

where A_1 corresponds to diagrams for which all the internal loops are formed by the same type of leptons as the external one; it also includes diagrams with exchanges of only one virtual photon without lepton loops. Clearly, the coefficients A_1 are universal for all kinds of leptons. The mass-dependent coefficients A_2 and A_3 include diagrams with leptons $\ell \neq L$.

In turn, each coefficient A_i can be developed in to the Taylor series w.r.t. $\left(\frac{\alpha}{\pi}\right)$

$$A_{1,L}(m_L/m_L) = A_{1,L}^{(2)}\left(\frac{\alpha}{\pi}\right)^1 + A_{1,L}^{(4)}\left(\frac{\alpha}{\pi}\right)^2 + A_{1,L}^{(6)}\left(\frac{\alpha}{\pi}\right)^3 + \cdots, \tag{13}$$

$$A_{2,L}\,(r = m_\ell/m_L) = A_{2,L}^{(4)}(r)\left(\frac{\alpha}{\pi}\right)^2 + A_{2,L}^{(6)}(r)\left(\frac{\alpha}{\pi}\right)^3 + A_{2,L}^{(8)}(r)\left(\frac{\alpha}{\pi}\right)^4 + \cdots, \tag{14}$$

$$A_{3,L}\,(r_1, r_2) = A_{3,L}^{(6)}(r_1, r_2)\left(\frac{\alpha}{\pi}\right)^3 + A_{3,L}^{(8)}(r_1, r_2)\left(\frac{\alpha}{\pi}\right)^4 + A_{3,L}^{(10)}(r_1, r_2)\left(\frac{\alpha}{\pi}\right)^5 + \cdots, \tag{15}$$

where $r = r_1 = m_{\ell_1}/m_L$, $r_2 = m_{\ell_2}/m_L$ and the superscripts of the coefficient in the r.h.s. indicate the corresponding order of the radiative corrections. As mentioned, the leading order correction to the lepton anomaly $a_L^{(0,0)} = \frac{\alpha}{2\pi}$ was calculated, for the first time, by J. S. Schwinger [2]. In our notation this corresponds to $A_{1,L}^{(2)} = 1/2$. The next coefficients $A_{1,L}^{(4)}$ and $A_{1,L}^{(6)}\ldots$ are also known explicitly up to an impressive large order of corrections (up to 13 loops, see e.g., [3, 24]).

Here below, we focus on further investigations of the mass-dependent coefficients $A_{2,L}^{(i)}(r)$ in Eq. (14) by means of the Mellin-Barns technique. Previously, in Refs. [13, 14] we considered the radiative corrections from diagrams consisting on only pure closed lepton loops, the so-called "bubble"-like diagrams. Now we complicating the task by including in to the consideration diagrams with loops crossed by internal photon lines, hereafter referred to as "mixed" diagrams, see Fig. 3. Hitherto, the exact analytical expressions for this type of diagrams were derived only for the universal coefficient $A_{1,L}^{(6)} = A_{2,L}^{(6)}(r = 1)$, see Refs. [25, 26],

$$\begin{aligned} A_{2,L}^{(6)}(1) \;&= \frac{673}{108} - \frac{41\pi^2}{81} - \frac{7\pi^4}{270} - \frac{4}{9}\,\pi^2\ln(2) - \frac{4}{9}\,\pi^2\ln^2(2) + \frac{4}{9}\ln^4(2) \\ &+ \frac{32}{3}\,\mathrm{Li}_4\left(\frac{1}{2}\right) + \frac{13\,\zeta(3)}{18} = 0.05287065\ldots, \end{aligned} \tag{16}$$

where Li_4 is the polylogarithm function of the order 4, $\mathrm{Li}_n(z) = \sum_{k=1}^{\infty}(z^k/k^n)$, and $\zeta(3)$ is the Riemann zeta function, $\zeta(z) = \sum_{k=1}^{\infty}(1/z^k)$.

So far, due to cumbersomeness of the explicit expressions of mixed diagrams (more that 150 terms for the graphs of Fig. 3, cf. Ref. [15]), the mass dependent coefficients $A_2^{(6)}(r)$ were studied theoretically only in the asymptotic limits $r \ll 1$ and $r \to \infty$ [15]. Also, the mass dependent coefficients $A_3^{(6)}(r_1, r_2)$, i.e. the diagrams with all three leptons different, were analysed only in these asymptotic limits, see Refs. [21, 27].

3. The sixth order corrections

The sixth order corrections are generated by powers of the irreducible operator $\Pi(k^2)$ which includes graphs of the second and fourth orders, i.e. the graphs b) and c) in Fig. 2. The contributions from graphs of the type b) were analyzed in details in Ref. [13]. The sought sixth order corrections to a_L from the mixed diagrams are determined by the irreducible graph c) referred in what follows to as $\Pi_4(k^2)$; the corresponding diagrams are depicted in Fig. 3, for which $p = 0$ and $j = 1$ (see also Refs. [4, 13, 28]). Correspondingly,

$$\Omega_0(s) = \int_0^1 dx\, x^{2s}(1-x)^{1-s} = \frac{\Gamma(2-s)\Gamma(1+2s)}{\Gamma(3+s)}, \tag{17}$$

$$R_1^{(4)}(s) = 2\int_0^1 \delta d\delta (1-\delta^2)^{s-1}\frac{1}{\pi}\mathrm{Im}\left[\Pi_4^{(\ell)}(\delta)\right] = \left(\frac{\alpha}{\pi}\right)^2 2\int_0^1 \delta d\delta (1-\delta^2)^{s-1}\rho^{(4)}(\delta), \tag{18}$$

where, for the sake of brevity, we introduced the notation

$$\left(\frac{\alpha}{\pi}\right)^2 \rho^{(4)}(\delta) = \frac{1}{\pi}\mathrm{Im}\left[\Pi_4^{(\ell)}(\delta)\right]. \tag{19}$$

The fourth order "mixed" polarization operator $\Pi_4^{(\ell)}(\delta)$ is well-known in the literature and explicitly can be found in, e.g. Refs. [4, 29, 30]

$$\begin{aligned}\rho^{(4)}(\delta) = {} & \left[\frac{11}{16} + \frac{11\delta^2}{24} - \frac{7\delta^4}{48} + \left(\frac{1}{2} + \frac{\delta^2}{3} - \frac{\delta^4}{6}\right)\ln\left(\frac{(1+\delta)^3}{8\delta^2}\right)\right]\ln\left(\frac{1+\delta}{1-\delta}\right) \\ & + \delta\left[\frac{5}{8} - \frac{3\delta^2}{8} - \left(\frac{1}{2} - \frac{\delta^2}{6}\right)\ln\left(\frac{64\delta^4}{(1-\delta^2)^3}\right)\right] \\ & + 2\left(\frac{1}{2} + \frac{\delta^2}{3} - \frac{\delta^4}{6}\right)\left[2\,\mathrm{Li}_2\left(\frac{1-\delta}{1+\delta}\right) + \mathrm{Li}_2\left(-\frac{1-\delta}{1+\delta}\right)\right]\Theta(1-\delta),\end{aligned} \tag{20}$$

where $\mathrm{Li}_2(x)$ denotes the dilogarithm function. Thus, the anomaly $a_L^{(6)}$ becomes

$$\begin{aligned}a_L^{(6)} = {} & \left(\frac{\alpha}{\pi}\right)\frac{1}{2\pi i}\int_{c-i\infty}^{c+i\infty} ds\, r^{-2s}\frac{\Gamma(s)\Gamma(1-s)\Gamma(2-s)\Gamma(1+2s)}{\Gamma(3+s)}\, R_1^{(4)}(s) = \\ & \left(\frac{\alpha}{\pi}\right)^3\frac{1}{2\pi i}\int_{c-i\infty}^{c+i\infty} ds\, r^{-2s}\frac{2\sqrt{\pi}(1-s)\Gamma(1-s)\Gamma(\frac{1}{2}+s)}{(1+s)(2+s)\sin(\pi s)} 2\int_0^1 \delta d\delta (1-\delta^2)^{s-1}\rho^{(4)}(\delta).\end{aligned} \tag{21}$$

With Eq. (21) the coefficient $A_2^{(6)}(r)$ in Eq. (14) defining the contribution to the sixth order corrections from the diagrams in Fig. 3 can be presented in the form

$$A_{2,L}^{(6)}(r) = \frac{1}{2\pi i}\int\limits_{c-i\infty}^{c+i\infty} ds\, r^{-2s}\frac{\sqrt{\pi}(1-s)\Gamma(1-s)\Gamma(\frac{1}{2}+s)}{(1+s)(2+s)\sin(\pi s)} 2\int\limits_0^1 d\delta\delta\,(1-\delta^2)^{s-1}\rho^{(4)}(\delta), \quad (22)$$

which, after carrying out integration over δ, can be re-written as

$$A_{2,L}^{(6)}(r) = \frac{1}{2\pi i}\int\limits_{c-i\infty}^{c+i\infty} ds\, r^{-2s}\mathcal{F}(s)\,, \quad (23)$$

where the integrand $\mathcal{F}(s)$ explicitly reads as

$$\begin{aligned}\mathcal{F}(s) = \frac{\pi^2(1-s)}{\sin^2(\pi s)}\Bigg\{ &-\frac{72+408s+852s^2+749s^3+199s^4-72s^5-36s^6}{6s^2(1+s)(2+s)^3(1+2s)^2(3+2s)} \\ &+\frac{\pi^2}{12}\left(\frac{4}{s}-\frac{1}{2+s}\right)\frac{\Gamma(\frac{1}{2}+s)}{\sqrt{\pi}(1+s)(2+s)\Gamma(s)} + \frac{2+3s}{3\,s\,(1+s)(2+s)^2(1+2s)} \\ &\times\left[\psi\left(s+1/2\right)-3\psi(s)-2\gamma_E+2\ln(2)\right] + \frac{1}{3(\frac{1}{2}+s)(2+s)} \\ &\times\left[\frac{-4}{1+s}\,{}_3F_2\left(\frac{1}{2},\frac{1}{2},1;\frac{3}{2},\frac{3}{2}+s;1\right) + \frac{s}{(\frac{3}{2}+s)(\frac{5}{2}+s)}\,{}_3F_2\left(\frac{1}{2},\frac{1}{2},1;\frac{3}{2},\frac{7}{2}+s;1\right)\right]\Bigg\}. \end{aligned} \quad (24)$$

Above $\gamma_E = 0.5772156649\ldots$ denotes the Euler's constant, $\psi(s)$ is the known polygamma function and ${}_pF_q(a_1,a_2,\ldots a_p;b_1,b_2,\ldots b_q;1)$ are the generalized hypergeometric functions of the argument $x=1$.

3.1. Direct numerical calculations

Prior to proceed with analytical calculations of the Mellin integral (23) with the integrand (24) by the Cauchy's residue theorem, we recall that for this particular case considered in the present paper, i.e. for $p=0$ and $j=1$, the coefficient $A_{2,L}^{(6)}(r)$ can be calculated numerically directly from the definition (6). In this case the x-direction integration in Eq. (3) or Eq. (6) can be carried out analytically providing for the coefficient $A_2^{(6)}(r)$ the following expression

$$A_{2,L}^{(6)}(r) = \int\limits_0^1 \frac{2\delta}{1-\delta^2}\,\widetilde{K}_2(\delta,r)\,\rho^{(4)}(\delta)\,d\delta, \quad (25)$$

where $\rho^{(4)}(\delta)$ is defined by Eq. (20) and $\widetilde{K}_2(\delta,r)$ is the result of integration over x in (3) with $t/m_L^2 = 4r^2/(1-\delta^2)$ (see also Refs. [4, 19]),

$$\begin{aligned}\widetilde{K}_2(\delta,r) = \frac{1}{2}\Bigg[1-\frac{8r^2}{1-\delta^2}-\frac{8r^2}{1-\delta^2}\left(1-\frac{2r^2}{1-\delta^2}\right)\ln\left(\frac{4r^2}{1-\delta^2}\right)\Bigg] \\ +\frac{1}{\sqrt{1-\frac{1-\delta^2}{r^2}}}\left[1-\frac{8r^2}{1-\delta^2}+\frac{8r^4}{(1-\delta^2)^2}\right]\ln\left(\frac{1-\sqrt{1-\frac{1-\delta^2}{r^2}}}{1+\sqrt{1-\frac{1-\delta^2}{r^2}}}\right). \end{aligned} \quad (26)$$

In principle, Eqs. (25) and (26) are already suitable for numerical calculation of $A_2^{(6)}(r)$. However, these expressions are not sufficiently convenient for, they do not allow further refinement investigations of the analytical properties of $A_{2,L}^{(6)}(r)$, e.g. the asymptotic behaviour at $r \to \infty$ or $r \ll 1$, dependence on the types of leptons in the loops, comparisons with results already reported in the literature etc. Such kind of analysis can be performed only if one has explicit analytical expressions of $A_{2,L}^{(6)}(r)$. Nevertheless, Eq. (25) can serve as an extremely useful tool for crosschecking the numerical results obtained from the exact, but rather cumbersome analytical expressions (see below).

Besides this possibility of numerical checks of the exact formulae, another way of testing the results is to compare the analytical expressions with those known in the literature. Later on we compute (numerically) the limit $r \to 1$ and compare with the explicit expression for $A_{2,L}^{(6)}(r = 1)$, Eq. (16). Also the limits $r \gg 1$ and $r \ll 1$ are employed for comparisons with known results [15].

3.2. Analytical calculations: right semi-plane $r > 1$

Having computed explicitly the integrand (24), the Mellin integral (23) can be calculated straightforwardly by means of the Cauchy's residue theorem closing the integration contour consecutively to the right ($r > 1$) and to the left ($r < 1$) semi-planes of the complex variable s. From Eq. (24) one infers that $\mathcal{F}(s)$ is a singular function in both semi-planes of s. So, in the right semi-plane ($r > 1$) the integrand $\mathcal{F}(s)$ possesses a pole of the first order at $s = 1$ and poles of the second order for positive integers $s > 1$, $s = 2, 3, \ldots n \ldots$. The residue at $s = 1$ is easily calculable

$$\mathrm{Res}\left[r^{-2s}\mathcal{F}(s)\right]_{s=1} = -\frac{41}{486}\frac{1}{r^2}. \tag{27}$$

The remaining poles, all of the second order, are located at integer $s > 1$, hence $A_2^{(6)}$ can be written as

$$A_{2,L}^{(6)}(r > 1) = \frac{41}{486}\frac{1}{r^2} - \sum_{n=2}^{\infty} \mathrm{Res}\left[r^{-2s}\mathcal{F}(s)\right]_{s=n}. \tag{28}$$

The minus sign in (28) originates from the fact that the integration contour is clockwise. The residues in $s = 2, 3 \ldots$ in Eq. (28) have been calculated by means of the available computer packages with ability of symbol manipulation. The result is

$$A_{2,L}^{(6)}(r > 1) = C_1(r) + C_2(r)\ln(r) + \left(\frac{7}{2} - 8r^2 - \frac{115}{18}r^4\right)\ln^2(r) + \Sigma(r), \tag{29}$$

where

$$C_1(r) = \frac{919}{144} + \frac{193}{1215r^2} - \frac{33}{4}r^2 + r\left(\frac{8}{9} + 10\,r^2\right)\left[\mathrm{Li}_2\left(\frac{1-r}{1+r}\right) - \mathrm{Li}_2\left(-\frac{1-r}{1+r}\right)\right]$$
$$-\frac{16}{9}r\left[\mathrm{Li}_3\left(\frac{1}{r}\right) - \mathrm{Li}_3\left(-\frac{1}{r}\right)\right] + \left(\frac{7}{4} - 4r^2 - \frac{115}{36}r^4\right)\left[2\mathrm{Li}_2\left(\frac{1-\frac{1}{r}}{1+\frac{1}{r}}\right) - 2\mathrm{Li}_2\left(-\frac{1-\frac{1}{r}}{1+\frac{1}{r}}\right)\right.$$
$$\left.+4\,\mathrm{Li}_2(1-r)\right] - \left(1 + \frac{4}{3}r^2 + \frac{23}{9}r^4\right)\mathrm{Li}_3\left(\frac{1}{r^2}\right) - 6\,r^4\mathrm{Li}_4\left(\frac{1}{r^2}\right) - \frac{\pi^2}{3}\left\{\frac{7}{8} - \frac{2}{3}r - 3r^2\right.$$
$$-\frac{15}{2}r^3 - \frac{5869}{72}r^4 + \frac{5984\,r^4 - 19232\,r^2 + 20388}{72\left(1-\frac{1}{r^2}\right)^{5/2}} - \frac{6854r^2 + 367}{72\,r^4\left(1-\frac{1}{r^2}\right)^{5/2}} + \frac{11}{144r^2}$$
$$-26r^2\left(1 + \frac{230}{39}r^2\right)\ln\left[\frac{1}{2}\left(1 + \sqrt{1-\frac{1}{r^2}}\right)\right] + 26r^2\,{}_4F_3\left(-\frac{1}{2}, 1, 1, 1; 2, 2, 2; \frac{1}{r^2}\right)$$
$$\left.-\frac{1}{54r^2}\,{}_4F_3\left(1, 1, \frac{3}{2}, 3; 4, 4, 4; \frac{1}{r^2}\right) + \frac{1}{9r^2}\,{}_6F_5\left(\frac{3}{2}, 3, 3, 3, 3, 3; 1, 1, 4, 4, 4; \frac{1}{r^2}\right)\right\}, \tag{30}$$

$$C_2(r) = 7 - \frac{127}{18}r^2 - \frac{8}{9}r\left[\mathrm{Li}_2\left(\frac{1}{r}\right) + \mathrm{Li}_2\left(-\frac{1}{r}\right)\right] - \left(1 + \frac{4}{3}r^2 + \frac{23}{9}r^4\right)\mathrm{Li}_2\left(\frac{1}{r^2}\right)$$
$$-4r^4\mathrm{Li}_3\left(\frac{1}{r^2}\right) - \frac{\pi^2}{3}\left\{1 - 10r^2 + \frac{206}{3}r^4 - \frac{53 - 259r^2 + 206r^4}{3\left(1-\frac{1}{r^2}\right)^{1/2}}\right.$$
$$\left.+ 48r^4\ln\left[\frac{1}{2}\left(1 + \sqrt{1-\frac{1}{r^2}}\right)\right] - 30r^2\,{}_3F_2\left(-\frac{1}{2}, 1, 1; 2, 2; \frac{1}{r^2}\right)\right\}, \tag{31}$$

$$\Sigma(r) = -\frac{8}{3}\sum_{n=2}^{\infty}\left\{\left[\frac{4n^3 + n^2 - 14n - 9}{(n+1)^2(n+2)(2n+1)}\,{}_3F_2\left(\frac{1}{2}, \frac{1}{2}, 1; \frac{3}{2}, \frac{3}{2} + n; 1\right)\right.\right.$$
$$\left.- \frac{16n^5 + 28n^4 - 104n^3 - 225n^2 - 60n + 30}{(n+2)(2n+1)(2n+3)^2(2n+5)^2}\,{}_3F_2\left(\frac{1}{2}, \frac{1}{2}, 1; \frac{3}{2}, \frac{7}{2} + n; 1\right)\right]$$
$$+ \frac{n-1}{n+1}\left[{}_3F_2\left(\frac{1}{2}, \frac{1}{2}, 1; \frac{3}{2}, \frac{3}{2} + n; 1\right) - \frac{n(n+1)}{(2n+3)(2n+5)}\,{}_3F_2\left(\frac{1}{2}, \frac{1}{2}, 1; \frac{3}{2}, \frac{7}{2} + n; 1\right)\right]$$
$$\times \ln(r^2) - \frac{n-1}{n+1}\left[\mathcal{X}\left(\frac{3}{2} + n\right) - \frac{n\,(n+1)}{(2n+3)(2n+5)}\,\mathcal{X}\left(\frac{7}{2} + n\right)\right]$$
$$- \frac{(n-1)(2n+1)(3n+8)\,\Gamma(n+1/2)\,\pi^{3/2}}{32\,(n+1)!(n+2)}\left(\psi(n) - \psi(n+1/2)\right) - \frac{(n-1)(3n+2)}{8n(n+1)(n+2)}$$
$$\times\left[3\,\psi^{(1)}(n) - \psi^{(1)}\,(n+1/2) - \left(3\psi(n) - \psi(n+1/2) + 2\gamma_E - 2\ln(2)\right)\ln(r^2)\right]$$
$$\left.- \frac{9n^5 + 11n^4 - 17n^3 - 31n^2 - 15n - 2}{4n^2(n+1)^2(n+2)^2(2n+1)}\right\}\frac{r^{-2n}}{(n+2)(2n+1)}. \tag{32}$$

The quantities $\mathcal{X}\left(n+\frac{3}{2}\right)$ and $\mathcal{X}\left(n+\frac{7}{2}\right)$ in Eq. (32) are the shorthand notation for the first derivatives of the hypergeometric function,

$$\mathcal{X}\left(\frac{3}{2}+n\right) \equiv \frac{\partial}{\partial s}\left[{}_3F_2\left(\frac{1}{2},\frac{1}{2},1;\frac{3}{2},\frac{3}{2}+s;1\right)\right]_{s=n}$$
$$= \sum_{k=0}^{\infty} \frac{\Gamma\left(\frac{1}{2}+k\right)}{\sqrt{\pi}\,(1+2k)} \frac{\Gamma\left(\frac{3}{2}+n\right)}{\Gamma\left(\frac{3}{2}+k+n\right)}\left[\psi\left(\frac{3}{2}+n\right)-\psi\left(\frac{3}{2}+n+k\right)\right]. \quad (33)$$

Explicitly, $\mathcal{X}\left(n+\frac{3}{2}\right)$ can be calculated from the integral representation of the corresponding hypergeometric function

$${}_3F_2\left(\frac{1}{2},\frac{1}{2},1;\frac{3}{2},s+\frac{3}{2};1\right) = -\frac{1}{\sqrt{\pi}}\frac{\Gamma\left(s+\frac{3}{2}\right)}{\Gamma\left(s+1\right)}\mathcal{I}(s), \quad (34)$$

where

$$\mathcal{I}(s) \equiv \int_0^1 \frac{dy}{y}(1-y^2)^s \ln\left[\frac{1-y}{1+y}\right]. \quad (35)$$

The derivatives $\mathcal{X}\left(n+\frac{7}{2}\right)$ in Eq. (32) can be related with $\mathcal{X}\left(n+\frac{3}{2}\right)$, Eq. (33), by merely shifting the argument by a factor of two, i.e. $\mathcal{X}\left(n+\frac{7}{2}\right) = \mathcal{X}\left((n+2)+\frac{3}{2}\right)$. With these results, the asymptotic of $A_2^{(6)}(r \gg 1)$, Eq. (29), reads as follows

$$A_{2,L}^{(6)}(r \gg 1) = \frac{41}{486}\frac{1}{r^2} + \frac{1}{r^4}\left(-\frac{449}{5400}\ln(r) - \frac{19871}{324000} + \frac{49}{768}\zeta(3)\right)$$
$$+ \frac{1}{r^6}\left(-\frac{62479}{661500}\ln(r) - \frac{665873}{8890560} + \frac{119}{1920}\zeta(3)\right)$$
$$+ \frac{1}{r^8}\left(\frac{25993}{291600}\ln(r) - \frac{19963}{293932800} - \frac{245}{4608}\zeta(3)\right) + \mathcal{O}\left(\frac{1}{r^{10}}\right), \quad (36)$$

which perfectly agrees with the expansion earlier reported in Ref. [15].

3.3. Analytical calculations: left semi-plane $r < 1$

The integration domain in Eq. (23) is specified by the strip $0 < c < 1$ where the corresponding hypergeometric functions are defined and are analytical functions. A more meticulous analysis of the functions ${}_3F_2\left(\frac{1}{2},\frac{1}{2},1;\frac{3}{2},\frac{3}{2}+s;1\right)$ and ${}_3F_2\left(\frac{1}{2},\frac{1}{2},1;\frac{3}{2},\frac{7}{2}+s;1\right)$ shows that they are valid in a larger region, namely in the complex plane $\mathrm{Re}\, s > -1$ and $\mathrm{Re}\, s > -3$, respectively, whereas outside this regions these functions are not defined at all. This can impede further evaluations of the integrals by the Cauchy's residue theorem in the left semi-plane of s. Therefore, an analytical continuation of these functions to the left semi-plane is necessary.

As seen from Eq. (24), in the left semi-plane the integrand $\mathcal{F}(s)$ possesses poles at negative integers $s = 0, -1, -2, ..., -n$ ... and negative half-integers $s = -\frac{1}{2}, -\frac{3}{2}, -\frac{5}{2}$. The residues in the poles $s = 0$ and $s = -1/2$ can be easily calculated

$$\mathrm{Res}\left[r^{-2s}\mathcal{F}(s)\right]_{s=0} = \frac{1}{4}\ln(r) + \frac{1}{2}\,\zeta(3) - \frac{5}{12}\,, \tag{37}$$

$$\mathrm{Res}\left[r^{-2s}\mathcal{F}(s)\right]_{s=-1/2} = \left(\frac{79}{27}\pi^2 - \frac{16}{9}\pi^2\ln(2) - \frac{13}{18}\pi^3\right) r. \tag{38}$$

To extend the definitions of the hypergeometric functions ${}_3F_2\left(\frac{1}{2},\frac{1}{2},1;\frac{3}{2},\frac{3}{2}+s;1\right)$ and of ${}_3F_2\left(\frac{1}{2},\frac{1}{2},1;\frac{3}{2},\frac{7}{2}+s;1\right)$ in the regions Re $s < -1$ and Re $s < -3$, respectively, the integral representations (34) and (35) can be used. Then, we get the desired analytical continuation of ${}_3F_2\left(\frac{1}{2},\frac{1}{2},1;\frac{3}{2},\frac{3}{2}+s;1\right)$ in the whole semi-plane Re $s < -1$ as

$${}_3F_2\left(\frac{1}{2},\frac{1}{2},1;\frac{3}{2},\frac{3}{2}+s;1\right)\Big|_{\mathrm{Re}\ s<-1} \Longrightarrow \frac{{}_3F_2\left(1,1+s,1+s;\frac{3}{2}+s,2+s;1\right)}{2(s+1)}\,. \tag{39}$$

Analytical continuation of ${}_3F_2\left(\frac{1}{2},\frac{1}{2},1;\frac{3}{2},\frac{7}{2}+s;1\right)$ follows immediately from Eq. (39) observing that ${}_3F_2\left(\frac{1}{2},\frac{1}{2},1;\frac{3}{2},\frac{7}{2}+s;1\right) = {}_3F_2\left(\frac{1}{2},\frac{1}{2},1;\frac{3}{2},\frac{3}{2}+(2+s);1\right)$, i.e.

$${}_3F_2\left(\frac{1}{2},\frac{1}{2},1;\frac{3}{2},\frac{7}{2}+s;1\right)\Big|_{\mathrm{Re}\ s<-3} \Longrightarrow \frac{1}{2(s+3)}{}_3F_2\left(1,3+s,3+s;s+4,\frac{7}{2}+s;1\right)\,. \tag{40}$$

Note that Eqs. (39) and (40) are fulfilled as exact identities for Re $s > -1$ and Re $s > -3$, respectively.

The last effort in preparing Eq. (24) for the Cauchy's integration in the left semi-plane is to express the corresponding hypergeometric functions (39) and (40) via the Pochhammer symbols $(a)_k$, viz.

$${}_3F_2\left(1,1+s,1+s;2+s,\frac{3}{2}+s;1\right) = \sum_{k=0}^{\infty}\frac{(s+1)_k}{(s+\frac{3}{2})_k}\,\frac{s+1}{k+s+1}\,, \tag{41}$$

where $(a)_k$, also known as the rising factorials, are defined as $(a)_k = \Gamma(a+k)/\Gamma(a)$. Notice that the Euler gamma functions in the definition of the Pochhammer symbols induce additional singularities in the left semi-plane. In turns, in counting the residues, these singularities give rise to double sums, over n and k in the final integration. All together, the integrand in the left semi-plane is singular with poles of different orders at negative integers $s = 0, -1, -2, -3, \ldots$ and negative half-integers $s = -1/2, -3/2, -5/2 \ldots$. Then $A_{2,L}^{(6)}(r)$ acquires the form

$$A_{2,L}^{(6)}(r) = \sum_{n=0}^{\infty}\mathrm{Res}\left[r^{-2s}\mathcal{F}(s)\right]_{s=-n} + \sum_{n=0}^{\infty}\mathrm{Res}\left[r^{-2s}\mathcal{F}(s)\right]_{s=-(2n+1)/2} \tag{42}$$

with the residues at $n = 0$ and $n = -1/2$ were already listed in Eqs. (37) and (38), respectively.

Eventually, explicit summations over all residues result in

$$A_{2,L}^{(6)}(r<1) = D_1(r) + D_2(r)\ln(r^2) + D_3(r)\ln^2(r) + 4r^4\ln^3(r) + \sum_{n=3}^{\infty} d_1(n,r)r^{2n} + \sum_{n=3}^{\infty} d_2(n,r)r^{2n} + \sum_{n=3}^{\infty}\sum_{k=0}^{n-2} d_3(n,k,r)r^{2n} + \sum_{n=4}^{\infty}\sum_{k=0}^{n-4} d_4(n,k,r)r^{2n} . \quad (43)$$

Since the explicit expression of $A_2^{(6)}(r<1)$, Eq. (43), is much more cumbersome in comparison with $A_2^{(6)}(r>1)$, defined by Eqs. (30)-(32), we do not present it here. We just stress that it includes a number of special functions, e.g. polylogarithms of different orders, inverse trigonometric and hyperbolic functions, polygamma's etc and polynomials of r. Explicitly, the coefficients $A_2^{(6)}(r)$ will be presented elsewhere. Herebelow we only compare the results of expansions of the exact expressions of $A_2^{(6)}(r)$ at small $r \ll 1$ with the known results early reported in the literature, cf. Ref. [15]. To reconcile our expansion with the Ref. [15], in summations over residues in Eq. (43), it is sufficient to consider only few first residues, $s = 0, -1, -2, -3$ and $s = -\frac{1}{2}, -\frac{3}{2}, -\frac{5}{2}$.

The result of the expansion about $r \sim 0$ is

$$A_{2,L}^{(6)}(r \ll 1) = -\frac{1}{4}\ln(r) + \frac{1}{2}\zeta(3) - \frac{5}{12} + \pi^2\left(\frac{79}{27} - \frac{13}{18}\pi - \frac{16}{9}\ln(2)\right)r + \left(6\ln^2(r) + 3\ln(r) + \frac{35}{3} + \pi^2 - 9\zeta(3)\right)r^2 + \pi^2\left(\frac{35}{12}\pi - \frac{50}{9}\right)r^3 + \left[4\ln^3(r) - \frac{27}{2}\ln^2(r) + \left(\frac{107}{4} + 2\pi^2 - 4\zeta(3)\right)\ln(r) - \frac{4}{9}\pi^2\ln^2(2) - \frac{5}{54}\pi^4 + \frac{32}{3}\mathrm{Li}_4\left(\frac{1}{2}\right) + \frac{4}{9}\ln^4(2) + 15\zeta(3) - \frac{9}{4}\pi^2 - \frac{3739}{144}\right]r^4 - \frac{7}{3}\pi^2\left(\frac{11}{15} - \frac{1}{16}\pi\right)r^5 + \left(\frac{116}{45}\ln^2(r) - \frac{1127}{225}\ln(r) + \frac{42343}{10125} + \frac{58\pi^2}{135}\right)r^6 + \mathcal{O}(r^7) . \quad (44)$$

Observe that the first terms, up to $\mathcal{O}\left(r^5\right)$, in Eq. (44) exactly reproduce the results of Ref. [15].

4. Numerical results

Herebelow we perform some checks of the validity of the obtained exact expressions by comparing results from Eqs. (43) and (29) with the corresponding direct numerical calculations of the integrals in Eqs. (25)-(26). We did such checks at several values of r and obtained excellent agreements between two methods of calculations. This persuades us of high confidence of the validity in our analytical results.

The behaviour of $A_{2,L}^{(6)}(r)$ in dependence on r is presented on Fig. 4. The solid curves reflect the results of calculations by the exact formulae, Eqs. (29)-(32), right panel, and by Eq. (43), left panel. The dashed curves are results of calculations of the asymptotic for $r > 1$, Eq. (36), and $r < 1$, Eq. (44), the right and left panels, respectively. The open circles, as well as the associated with them labels A_L^{ℓ}, point to physical values of $A_{2,L}^{(6)}(r)$ at the physical lepton mass ratios $r = m_\ell/m_L$. In our actual calculations these

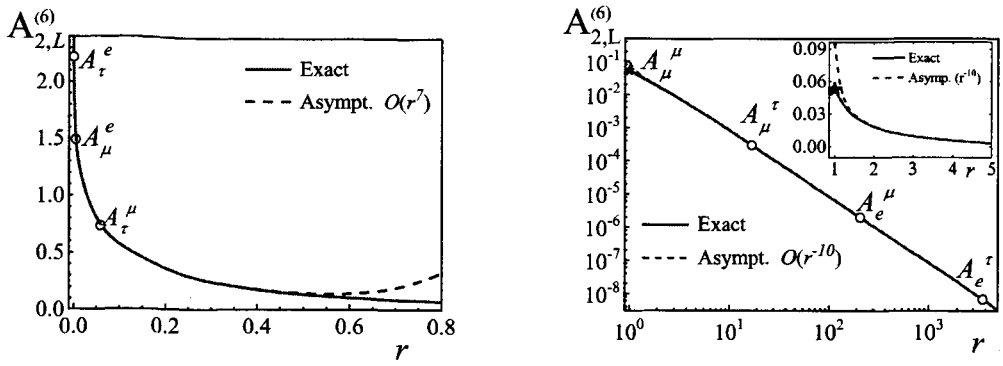

Figure 4: The sixth order corrections $A^{(6)}_{2,L}(r)$ to the lepton anomaly due to insertions of the fourth order polarization operator with one internal photon line. Solid curves correspond to calculations by exact analytical expressions, dashed curves are results of calculations by asymptotic expansion, Eq. (44) for the left panel and Eq. (36) for the right panel. The open circles, as well as the associated with them labels A^ℓ_L, point to physical values of $A^{(6)}_{2,L}(r)$ at the physical ratio $r = m_\ell/m_L$. The star corresponds to the universal value of $A^{(6)}_{2,L}(r=1)$. For a better vision of the behaviour at small r, the magnified area $1 < r < 5$ is highlighted in the upper corner where the linear scale for both axes is employed.

ratios correspond to those recommended by the International Committee on DATA (CODATA 2018) [31], namely: $m_e/m_\tau = 0.000287585(19)$, $m_e/m_\mu = 0.00483633169(11)$, $m_\mu/m_\tau = 0.0594635(40)$, $m_\tau/m_\mu = 16.8170(11)$, $m_\mu/m_e = 206.7682830(46)$ and $m_\tau/m_e = 3477.23(23)$.

From the Fig. 4 and from the corresponding numerical analysis, one can conclude that the exact analytical results practically coincide with the results by approximate formulae (44) in the interval $0 < r < 0.1$ and by Eq. (36) in the interval $2 < r < \infty$, respectively.

More precisely, the validity of the asymptotic expansions and the limits of their applicability can be illustrated if one defines the relative deviation $\varepsilon_L(r)$ of the approximate calculations from the exact results as

$$\varepsilon_L(r) = \frac{\left|A^{(6)}_{2,L\ asymp.}(r) - A^{(6)}_{2,L\ exact}(r)\right|}{A^{(6)}_{2,L\ exact}(r)}.$$

Then for, e.g., the muon anomaly, the maximum contribution is from the fourth order electron vacuum polarization operator. In this case ($L = \mu$ and $\ell = e$) $A^{(6)}_{2,L\ exact}(r_e) \simeq 1.49367182340837205$, whereas Eq. (44) keeping terms up to $\mathcal{O}(r^4)$ (this approximation corresponds to the one reported in Ref. [16]) result in $A^{(6)}_{2,L\ asymp}\big(\mathcal{O}(r^4)\big) = 1.49367182344$. In terms of the relative errors $\varepsilon_\mu(r_e)$ this corresponds to $\varepsilon_\mu(r_e)\big(\mathcal{O}(r^4)\big) \approx 2.1 \cdot 10^{-11}$. The relative errors rapidly decrease if in Eq. (44) one keeps terms up to $\mathcal{O}(r^6)$. In this case $A^{(6)}_{2,L\ asymp}\big(\mathcal{O}(r^6)\big) = 1.49367182340837220$ and consequently, $\varepsilon_\mu(r_e)\big(\mathcal{O}(r^6)\big) \approx 1.0 \cdot 10^{-16}$. Hence, in calculations of the corrections from electron loops to the muon anomaly it is quite sufficient to restrict oneself to terms $\sim \mathcal{O}(r^4)$ which assure accuracies higher than the experimental errors related to the measured [31] ratio of electron to muon masses $\Delta r \sim 10^{-10}$. To estimate how far from $r \to 0$ one can apply the approximate formula, Eq. (44), we compare the exact results with the expansions $\sim \mathcal{O}(r^4)$ and $\sim \mathcal{O}(r^6)$ at

$r = 0.1$. We obtained that keeping terms $\sim \mathcal{O}(r^4)$, Eq. (44) assures only four significant digits while keeping terms $\sim \mathcal{O}(r^6)$, the approximate formula provides much more accurate results, namely up to seven significant digits in the interval $(0 < r < 0.1)$. This accuracy is above the experimental measurements in this interval. An analogous situation occurs also in the region $r > 2$, cf. Table 1.

Table 1: The relative deviation $\varepsilon(r)$ of the asymptotic results from the exact calculations at r corresponding to the really existing leptons [31]

r	$r<1$			$r>1$			
mass ratio	e/τ	e/μ	μ/τ	mass ratio	τ/μ	μ/e	τ/e
r	0.00028759	0.0048363	0.0594635	r	16.8170	206.768	3477.23
$\mathcal{O}(r^4)$	$1.1\cdot10^{-17}$	$2.1\cdot10^{-11}$	$1.0\cdot10^{-5}$	$\mathcal{O}(r^{-8})$	$1.4\cdot10^{-7}$	$7.3\cdot10^{-14}$	$4.9\cdot10^{-21}$
$\mathcal{O}(r^6)$	$1.9\cdot10^{-25}$	$1.1\cdot10^{-16}$	$7.3\cdot10^{-9}$	$\mathcal{O}(r^{-10})$	$3.6\cdot10^{-8}$	$1.1\cdot10^{-14}$	$4.5\cdot10^{-22}$

It should be noted that the sums, Eqs. (32) and (43), in the analytical expression are rather poorly convergent when $r \to 1$. Consequently, for reliable calculations it is required to take into account a large number, several hundreds or even thousands, of terms in the sums. For instance, at $r = 2$ to assure the value $A_{2,L}^{(6)}(2) \approx 0.017086812024867475167$ it is sufficient to take into account ~ 30 terms. The situation is worsening as $r \to 1$, where to assure only three significant digits in comparison with the calculations by Eq. (16), one already needs ~ 150 terms, whereas for a reliable accuracy more than one thousand terms are necessary.

Finally, we shall discuss the contribution of other sixth order corrections to $A_{2,L}^{(6)}(r)$ from insertions of the fourth order polarization operators. As mentioned, besides diagrams defined in Fig. 3 , there is another type of the fourth order polarization operators, namely the operator consisting on two closed lepton loops as depicted in Fig. 2b.

This type of corrections has been thoroughly studied in Ref. [13], where contributions of all possible combinations of internal and external types of leptons were investigated for polarization operators with two and three closed lepton loops. In Fig. 5 the contribution of different kind of the polarization operators is presented, where the solid curve is the coefficient $A_2^{(6)}(r)$ due to mixed diagrams, dashed and dot-dashed lines are the corrections from the pure bubble-like polarization operators with insertions of two identical $(\ell\ell)$ loops and two loops with different leptons $(L\ell)$. In the region $r < 1$ the main contribution to heavier lepton, τ and μ, comes from insertions of two identical electron loops. The contribution of bubble-like diagrams with one heavy lepton (dot-dashed line in Fig. 5, $r < 1$) is by far smaller than other contributions. The role of mixed loops increases with increase of r.

A different situation is in the right semi-plane $r \geq 1$, where the mixed diagrams are predominant.

5. Summary

In summary, we have presented, for the first time, exact analytical expressions for the sixth order radiative corrections to the anomalous magnetic moments of leptons e, μ and τ induced by Feynman diagrams with insertions of the fourth order vacuum polarization operator with one lepton loop crossed by one internal photon line. The approach essentially relies on the dispersion relations and the Mellin-Barnes transform for the propagators of massive photons previously employed in calculations of the pure bubble-like diagrams.

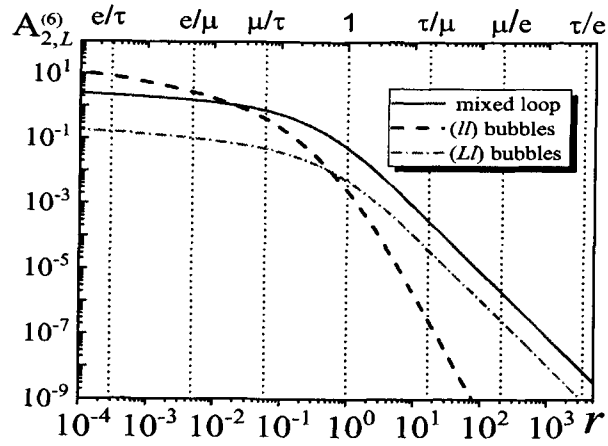

Figure 5: The sixth order corrections $A_{2,L}^{(6)}(r)$ to the lepton anomaly due to insertions of the fourth order polarization operator: solid line corresponds to one loop polarization operator with one internal photon line, dashed and dot-dashed lines correspond to insertions of the pure two-bubble loops operators with two identical $(\ell\ell)$ and two different $(L\ell)$ closed lepton loops, respectively, cf. Ref. [13]. The vertical lines, labeled according to the ratios $r = m_\ell/m_L$, indicate the values r of the physically existing leptons.

This method allows one to derive explicitly the corresponding sixth order corrections $a_L(r)$ as functions of the ratio $r = m_\ell/m_L$ of the mass of the internal ℓ to the mass of the external L leptons in the whole interval $(0 < r < \infty)$. It is argued that for every type of leptons the main contribution to $a_L(r)$ is provided by insertions of the polarization operator with leptons ℓ in the loop lighter than the external lepton L, c.f. labels in Figs. 4 and 5. Since for real existing leptons one has either $r \ll 1$ ($r_{max} \lesssim 0.06$), or $r \gg 1$ ($r_{min} \gtrsim 16$), the exact expressions can be safely substituted by their asymptotic expansions, which are much simpler and more convenient for numerical calculations. We affirm that these expansions work quite well in the intervals $(0 < r < 0.1)$ and $(2 < r < \infty)$ within which the physical ratios $r = m_\ell/m_L$ are located. We investigated the limits of applicability of the asymptotic expansions and claim that with a reasonable number of terms these asymptotics are quite appropriate for practical numerical calculations.

6. Acknowledgments

This work was supported in part by a grant under the Belarus–JINR scientific collaboration. A bulk of numerical calculations were performed on the basis of the HybriLIT heterogeneous computing platform (supercomputer "Govorun" , LIT, JINR). Useful discussions with Prof. A.V. Kotikov are gratefully acknowledged.

References

[1] P. A. M. Dirac, The quantum theory of the electron, Proc. Roy. Soc. Lond. A **117**, 619 (1928).

[2] J. S. Schwinger, On Quantum electrodynamics and the magnetic moment of the electron, Phys. Rev. **73**, 416 (1948); Quantum electrodynamics. III: The electromagnetic properties of the electron: radiative corrections to scattering, Phys. Rev. **76**, 790 (1949).

[3] F. Jegerlehner, The anomalous magnetic moment of the muon, Springer Tracts Mod. Phys. **274**, 693 (2017).

[4] B. E. Lautrup and E. de Rafael, Calculation of the sixth-order contribution from the fourth-order vacuum polarization to the difference of the anomalous magnetic moments of muon and electron, Phys. Rev. **174**, 1835 (1968).

[5] R. Aliberti,T. Aoyama, E. Balzani et al, The anomalous magnetic moment of the muon in the Standard Model: an update, arXiv:2505.21476v1 [hep-ph] May 2025.

[6] J. Charles, E. de Rafael, D. Greynat, Mellin-Barnes approach to hadronic vacuum polarization and $g_\mu - 2$, Phys. Rev. D **97**, 076014 (2018).

[7] I. Dubovyk, J. Gluza and G. Somogyi, Mellin-Barnes Integrals: A Primer on Particle Physics Applications, Lect. Notes Phys. **1008**, 208 (2022).

[8] S. Laporta, High-precision calculations of multiloop Feynman integrals by difference equations, J. Mod. Phys. **A 15**, 5087 (2000).

[9] S. Laporta, High-precision calculations of the 4-loop contribution to the electron $g - 2$ in QED, Phys. Lett. **B 772**, 332 (2017).

[10] D. H. Bailey and D.J. Broadhurst, Parallel integer relation detection: techniques and applications, Math. Comp. **70**, 1719 (2000).

[11] S. Friot, D. Greynat, On convergent series representations of Mellin-Barnes integrals, J. Math. Phys. **53**, 023508 (2012).

[12] B. Ananthanarayan, S. Friot, S. Ghosh, Three-loop QED contributions to the $g - 2$ of charged leptons with two internal fermion loops and a class of Kampe de Feriet series, Phys. Rev. D **101**, 116008 (2020).

[13] O.P. Solovtsova, V. I.Lashkevich, L. P.Kaptari, Lepton anomaly from QED diagrams with vacuum polarization insertions within the Mellin– Barnes representation. Eur. Phys. J. Plus D **138**, 212 (2023).

[14] O. P. Solovtsova, V. I.Lashkevich, L. P. Kaptari. Analytical calculations of the tenth order QED radiative corrections to lepton anomalies within the Mellin–Barnes representation. Journal of Physics G: Nuclear and Particle Physics **51**, 055001 (2024).

[15] S. Laporta, The analytical contribution of the sixth order graphs with vacuum polarization insertions to the muon $(g - 2)$ in QED, Nuovo Cim. A **106**, 675 (1993).

[16] J. P. Aguilar, E. de Rafael, D. Greynat, Muon anomaly from lepton vacuum polarization and the Mellin-Barnes representation, Phys. Rev. D **77**, 093010 (2008).

[17] R. Barbieri, E. Remiddi, Electron and muon $\frac{1}{2}(g - 2)$ from vacuum polarision insertions, Nucl. Phys. B **90**, 233 (1975).

[18] V. B. Berestetskii, O. N. Krohnin, A. K. Khlebnikov, Concerning the radiative corrections to the μ-meson magnetic moment, Zh. Eksp. Teor. Fiz. **30**, 788 (1956) [Sov. Phys. JETP, **3**, 761 (1956)].

[19] S. J. Brodsky, E. de Rafael, Suggested boson-lepton pair coupling and the anamalous magnetic moment of the muon, Phys. Rev. **168**, 1620 (1968).

[20] E. E. Boos and A. I. Davydychev, A method of evaluation massive Feynman diagrams, Theor. Math. Phys. **89**, 1052 (1991).

[21] S. Friot, D. Greynat, E. de Rafael, Asymptotics of Feynman diagrams and the Mellin-Barnes representation, Phys. Lett. B. **628**, 73 (2005).

[22] T. L. Trueman and T. Yao, High energy scattering amplitude in perturbation theory, Phys. Rev. **132**, 2741 (1963).

[23] T. Kinoshita, B. Nizic and Y. Okamoto, Eighth order QED contribution to the anomalous magnetic moment of the muon, Phys. Rev. D **41**, 593 (1990).

[24] M. L. Laursen, M. A. Samuel, The n-bubble diagram contribution to $(g-2)$ of the electron. Mathematical structure of the analytical expression, Phys. Letts. B **91**, 249 (1980);
M. L. Laursen, M. A. Samuel, Borel transform technique and the n bubble diagram contribution to the lepton anomaly, Phys. Rev. D **23**, 2478 (1981).

[25] S. Laporta and E. Remiddi, Analytic QED calculations of the anomalous magnetic moment of the electron, Adv. Ser. Direct. High Energy Phys. **20**, 119 (2009); doi:10.1142/9789814271844_0004

[26] J. A. Mignaco, E. Remiddi, Fourth-order vacuum polarization contribution to the sixth-order electron magnetic moment, Nouvo Cimento A **60**, 519 (1969).

[27] A. Czarnecki and M. Skrzypek, The Muon anomalous magnetic moment in QED: Three loop electron and tau contributions, Phys. Lett. **B 449**, 354 (1999).

[28] R. Barbieri, E. Remiddi, Infra-red divergences and adiabatic switching. Fourth-order vaccum polarization. Nouvo Cimento. A **13**, 99 (1973).

[29] M. Laursen and M. A. Samuel, Corrections to the sixth order anomalous magnetic moment of the muon, Phys. Rev. D **19**, 1281 (1979); doi:10.1103/PhysRevD.19.1281

[30] G.Källen, A. Sabry, Fourth order vacuum polarizatioln, Dan. Mat. Fys. Medd. **29**, no. 17, 556 (1955).

[31] E. Tiesinga, P.J. Mohr, D.B. Nevell, B.N. Taylor, CODATA recommended values of the fundamental physical constants: 2018. Reviews of Modern Physics **93**, art. ID 025010 (2021); https://doi.org/10.1103/RevModPhys.93.025010.